An Eight-User Time-Slotted SPECTS O-CDMA Testbed: Demonstration and Simulations

Ryan P. Scott, Wei Cong, Vincent J. Hernandez, Kebin Li, Brian H. Kolner, *Senior Member, IEEE*,
Jonathan P. Heritage, *Fellow, IEEE, Fellow, OSA*, and S. J. Ben Yoo, *Senior Member, IEEE, Member, OSA*

Abstract—This paper demonstrates an eight-user 9 Gb/s/user time-slotted spectral phase-encoded time-spreading (SPECTS) optical code division multiple access (O-CDMA) testbed. Experimentally measured performance is compared to numerical simulations. The testbed employs a novel compact fiber-pigtailed bulk-optics setup that utilizes a single two-dimensional (2-D) phase modulator for encoding multiple channels, each with a unique 64-chip Walsh code. The time-gated receiver is composed of a nonlinear optical loop mirror (NOLM) and a nonlinear thresholder each utilizing a highly nonlinear fiber (HNLF) as the nonlinear element. The testbed operates error free with up to six users and at a bit error rate BER $< 10^{-9}$ for eight simultaneous users. Careful modeling of each component in the testbed allows a close match between simulated and experimentally measured testbed performance.

Index Terms—Access networks, multiaccess communication, nonlinear detection, optical code division multiple access, optical fiber communications.

I. INTRODUCTION

OPTICAL CODE DIVISION multiple access (O-CDMA) technologies are currently being explored for use in local area networks [1], [2]. Code-based access of optical networks can potentially simplify network control and management when used in place of time division multiplexing (TDM) or wavelength division multiplexing (WDM) technologies. Without relying on complex distribution nodes for access, O-CDMA allows for the flexible allocation of the large bandwidth available in optical networks. Various implementations of O-CDMA have been proposed over the last 18 years, including both one-dimensional (1-D) [3]–[6] and two-dimensional (2-D) [7]–[9] codes. As the name implies, 1-D codes are applied solely in the temporal or spectral domain with the code spread across some number of chips. Alternatively, 2-D codes occupy both domains and are typically referred to as wavelength-time codes. In either case, the codes are chosen to have the most favorable cross-correlation and autocorrelation characteristics in order to minimize channel crosstalk, also known as multiaccess interference (MAI) or multiuser interference (MUI).

This paper investigates 1-D codes applied in the spectral domain called spectral phase-encoded time-spreading (SPECTS) O-CDMA [10]. In SPECTS O-CDMA, encoding is accomplished by phase shifting individual slices (i.e., chips) of a pulse's optical spectrum [11], [12]. The SPECTS codes are binary, with either a 0 or a π phase shift on each chip. This spectral phase shifting causes the pulse to spread in time by an amount proportional to the code size. To correctly retrieve a pulse, a decoder applies the conjugate of the encoding code, thus reconstructing the short pulse. The code sets are quasi-orthogonal, and if decoded using another code from the set, the pulse remains spread in time. A typical receiver, with a data-rate-limited bandwidth, will not distinguish between the correctly and incorrectly decoded pulses since each has comparable energy within a bit period. Therefore, it is necessary to use either a short time gate to select out the correctly decoded pulse or a nonlinear detector that responds to the larger peak power of a correctly decoded pulse. Some 1-D, and many 2-D, O-CDMA codes rely on direct-sequence encoding (i.e., each bit is represented by a sequence of short pulses), which means that the chip rate is always greater than the user's data rate, in many cases by an order of magnitude. Since SPECTS O-CDMA does not depend on direct-sequence encoding, it is data rate transparent and directly scales to high data rates. Therefore, SPECTS is one of the more promising O-CDMA technologies for future high-speed access networks that may operate at hundreds of gigabits or even terabit rates.

This paper presents a synchronous time-slotted SPECTS O-CDMA testbed with eight simultaneous users (four per time slot) each operating at 9 Gb/s. Although asynchronous operation would be preferred, coherent interference (arising from a single laser source) and MUI effects compel the use of a synchronous testbed. Synchronous operation provides several advantages including the ability to use time slots. Slotted operation increases the spectral efficiency for a given data rate and allows code reuse (i.e., the same code can be used in different time slots), thus increasing the possible number of simultaneous users for a given code size. Previous works [10], [13] relied on a highly nonlinear fiber (HNLF)-based thresholder [14] to suppress MUI. For the time-slotted testbed, gated detection becomes necessary, and this paper discusses two types: an ultrafast nonlinear interferometer (UNI) and a nonlinear optical loop mirror (NOLM) time gate. Section III discusses the operation and characteristics of both types. (Note: Jiang *et al.* have recently demonstrated slot-level timing coordination by

use of double coding and nonlinear optical processing [15], and Etemad *et al.* have demonstrated a four-user O-CDMA experiment using a semiconductor optical amplifier (SOA)-based terahertz optical asymmetric demultiplexer (TOAD) operating as a time gate [12].) While currently using both gating and nonlinear thresholding in this testbed, the authors are working to determine if the nonlinear thresholder can be eliminated. Section IV shows the bit error rate (BER) statistics of the testbed with each of the time gates for up to eight simultaneous users. The testbed is able to achieve error-free operation for up to six users and a BER $< 10^{-9}$ for eight users. Finally, Section V shows a simulation study of the testbed that confirms the experimental data. RSoft's OptSim software allows us to create detailed and accurate models for the test-bed components and provides reasonable agreement between experimental and simulation data for time-domain waveforms and BER performance.

II. TESTBED DESCRIPTION

The SPECTS O-CDMA testbed uses a zero-dispersion pulse shaper [16], [17], implemented in bulk optics with fiber pig-tails, for the encoders and decoder. To facilitate a relatively large number of users with a small table footprint, we utilized a reflective 2-D liquid-crystal spatial light phase modulator (LC-SLPM) (Hamamatsu X8267-1.5M) [18]. The active area of the LC-SLPM is 20×20 mm (768×768 pixels) and is optically addressed via the green value of an XGA monitor output signal from a personal computer. A total phase modulation range of 2π at 1550 nm is spread across 256 levels.

Fig. 1 shows the bulk optics arrangement for the pulse shapers. Cylindrical optics and long working distance collimators allow for the vertical stacking of individual channels. A cylindrical-optic telescope horizontally expands the beams to nearly cover the width of a 50-mm-wide 1100-line/mm grating. A 300-mm focal length plano-convex cylindrical lens is used to focus the individual spectral components onto the LC-SLPM. The spectral resolution of the pulse shaper is measured to be $\lesssim 0.1$ nm and is mainly limited by spherical aberrations from the simple cylindrical optics and diffraction effects from the miniature collimators. The 20-mm height of the LC-SLPM facilitates vertically stacking the five channels with a center-to-center spacing of ~ 4.5 mm. Each spectral chip occupies six pixels and a 64-chip code extends across a ~ 12.5-nm bandwidth. Currently, the total insertion loss for an individual channel, including circulators, is 10–13 dB.

A diagram of the eight-user time-slotted SPECTS O-CDMA testbed is shown in Fig. 2. A single laser source running at 9 Gb/s (111-ps period) is used to generate all of the various users and also the wavelength-shifted control pulse that is used to gate the intended user from the desired time slot. The laser source consists of a mode-locked fiber laser (PriTel UOC-3), producing 2.5-ps pulses, centered at 1550 nm, which are amplified (PriTel FA-27) and then compressed by a dispersion-decreasing fiber (PriTel PP-400) to 400 fs [~ 8 nm, full-width at half-maximum (FWHM)]. This pulse stream is modulated with a $2^{31} - 1$ pseudorandom bit sequence (PRBS) before it is multiplexed into two time slots (doubling the bit rate). The time
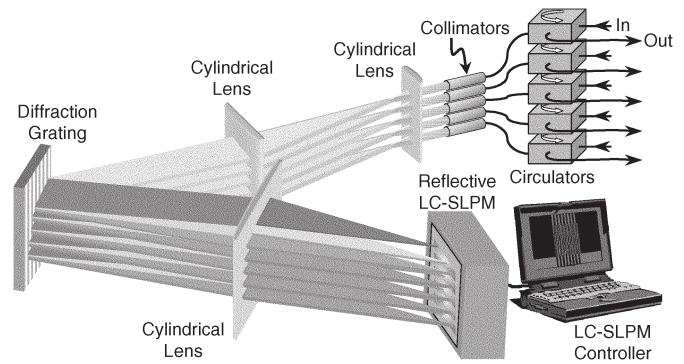

Fig. 1. Perspective view of the encoders/decoder as implemented in bulk optics.

multiplexer (MUX) splits the pulse stream and recombines it with a differential delay between the two paths of $(n + 1/2) \times$ input period, thus creating two interleaved time slots each 55.5-ps wide. In the testbed's time MUX, the integer n is large, leading to over 15 ns of differential delay that partially decorrelates the data in one time slot with respect to the other. After amplification by a dispersion-compensated erbium-doped fiber amplifier (DC-EDFA), the 2×9 Gb/s data stream is split into four separate channels, each with its own encoder. Encoders 1–4 each applies a different 64-chip Walsh code (5, 54, 52, and 32, respectively, see Table I) to their respective data streams and the decoder applies a code that is the conjugate of Encoder 1. Therefore, the data from Encoder 1 will be correctly decoded (intended user) and the data from other encoders will be incorrectly decoded (interfering users). Variable optical time delays are used to slot align each user to better than ± 1 ps and variable attenuators are used to equalize the users' powers within ± 0.2 dB. After combining, the differential delay between the various channels is typically 3–5 bits. A DC-EDFA ($+15$ dBm output) compensates for splitting/combining losses and the encoder losses before the signals go on to the decoder. Due to excess dispersion from the modulator along with residual dispersion and spectral narrowing in encoders and decoder, the decoder's output pulse width is typically 750–800 fs. In this setup, a NOLM is used to gate one of the time slots before the nonlinear thresholder. A detailed description of the NOLM operation is given in Section III. From an operational stand-point, the NOLM gate window is ~ 3 ps (FWHM) and provides nearly 20 dB of suppression outside the window. The pulse from the intended user is then passed through a low-noise DC-EDFA before going to the nonlinear thresholder. The thresholder uses a power DC-EDFA to amplify the signal before it goes into 500 m of HNLF (Sumitomo HNLF 1322AA-2). If the user's pulse has been correctly decoded, the high peak power of the short pulse generates spectra at longer and shorter wavelengths due to self-phase modulation (SPM) and other nonlinear effects in the HNLF. A long-pass filter then passes wavelengths longer than 1578 nm to the optical to electrical (O/E) converter. The lower peak power of the incorrectly decoded pulses will not generate much additional spectra and will be largely blocked by the long-pass filter. The typical power contrast ratio between correctly and incorrectly decoded pulses is better than 20 dB. For additional details of the thresholder
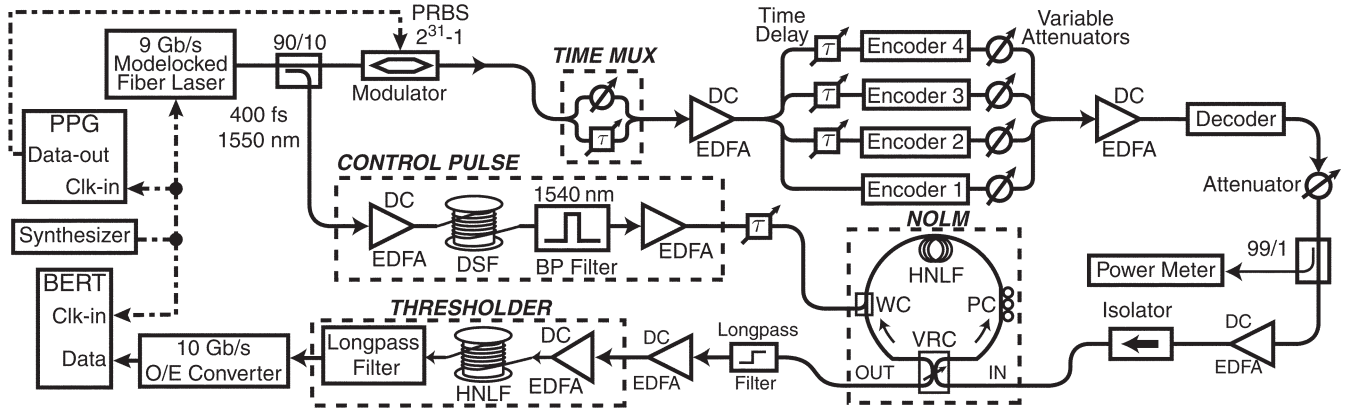
Fig. 2.   Diagram of the eight-user slotted SPECTS O-CDMA testbed. PPG: pseudorandom pattern generator. BERT: BER test set.

TABLE I
64-Chip Walsh Codes Used in the Testbed

Code Number	Code Listing (1 represents a π phase shift, 0 represents no phase shift)
5	1111 0000 1111 0000 1111 0000 1111 0000 1111 0000 1111 0000 1111 0000 1111 0000
54	1010 0101 1010 0101 0101 1010 0101 1010 0101 1010 0101 1010 1010 0101 1010 0101
52	1001 1001 1001 1001 0110 0110 0110 0110 0110 0110 0110 0110 1001 1001 1001 1001
32	1001 0110 0110 1001 0110 1001 1001 0110 1001 0110 0110 1001 0110 1001 1001 0110

operation, see [10] and [13]. During initial measurements of the testbed at 10 Gb/s, $\sim 4\%$ spurious reflections were discovered coming from the first surface of the LC-SLPM at ± 49 ps from the incident pulse. These spurious pulses were coherently interfering with the pulse at the center of the second time slot (± 50 ps), degrading the performance of the time-slotted testbed. To reduce the impact of this problem on our testbed measurements, we run the testbed at 9 Gb/s.

Since the pulses are short and the encoders are polarization sensitive (e.g., gratings and LC-SLPM in pulse shaper), we use a polarization-maintaining dispersion-shifted fiber (PM-DSF) for interconnecting components up to, and including, the decoder. After the decoder, DSF is generally used for connections. We use DSF for simplicity; however, it would be just as valid to use standard SMF-28 and then dispersion compensate the various sections of the testbed.

Walsh codes are chosen because of their property of spreading pulses such that the energy at the pulse center is minimized. Section V will show some simulated and measured time-domain waveforms that demonstrate this characteristic (note: the product of two Walsh codes is another Walsh code). In a synchronous testbed, the lack of energy at pulse center reduces the interference between the spread pulses and the correctly decoded user within the gate window. The amount that the pulse spreads when encoded is proportional to the length of the code, and longer codes are generally desired to minimize MUI. However, longer codes demand either higher encoder spectral resolution or more pulse bandwidth. As a compromise, we use 64-chip Walsh codes (0.2 nm/chip) that typically spread the pulse to a width of 50–60 ps and thus maximize the spreading but do not severely overfill the time slot or exceed the encoder's resolution. The particular Walsh codes that we use (5, 54, 52, and 32) were picked because each spreads the pulse out in a slightly different manner,

resulting in a moderately even distribution of energy from the interferers. This set of codes is probably representative of a less demanding scenario compared to one in which the code set amasses all of the interferers' energy near the center of the time slot. A more thorough study of code selection is beyond the scope of this paper and is saved for future work.

III. Gated Detection

To implement a time-slotted testbed, it is necessary to gate out the intended user's slot at the user's bit rate and reject the other time slot with adequate contrast. In fact, if the gate can be made sufficiently short, additional benefit can be realized by rejecting most of the energy from interfering users. Many optical gating techniques have been explored in the literature, including the UNI [19], the TOAD [20], and the NOLM [21], and some have even been applied to various O-CDMA schemes [12], [21], [22]. In the testbed, we have tried both a UNI and a NOLM as the gate. This section briefly describes the UNI operation and results and then, in more detail, the operation and results of the NOLM.

A. UNI Time Gate

Fig. 3 illustrates the operation of the UNI time gate. The input signal to the UNI is linearly polarized and separates into fast and slow components when launched at 45° with respect to the fast and slow axes of 4.5 m of PM-DSF. The two components, which have been separated by 6 ps, are sent to an SOA that serves as a nonlinear medium for time gating. A control pulse at a different wavelength is coincident with the slow component of the desired signal, inducing cross-phase modulation (XPM) inside the SOA and a π phase shift is imparted onto the slow component. Following the SOA, the fast and slow components
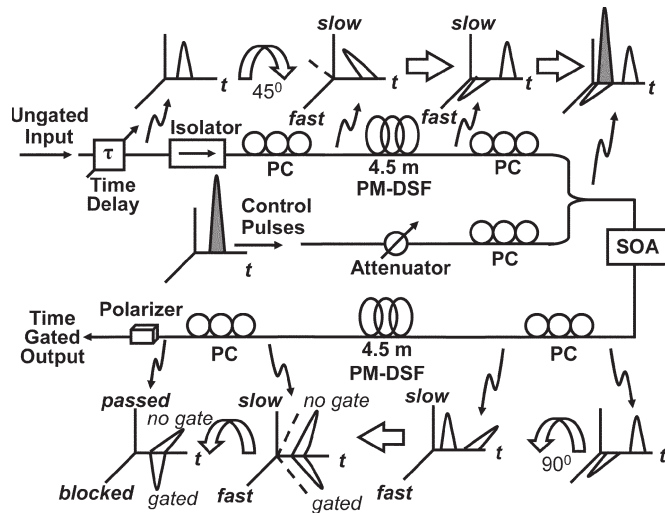
Fig. 3. Diagram showing the operating principle of the UNI time gate. Control pulse generation shown in Fig. 2.
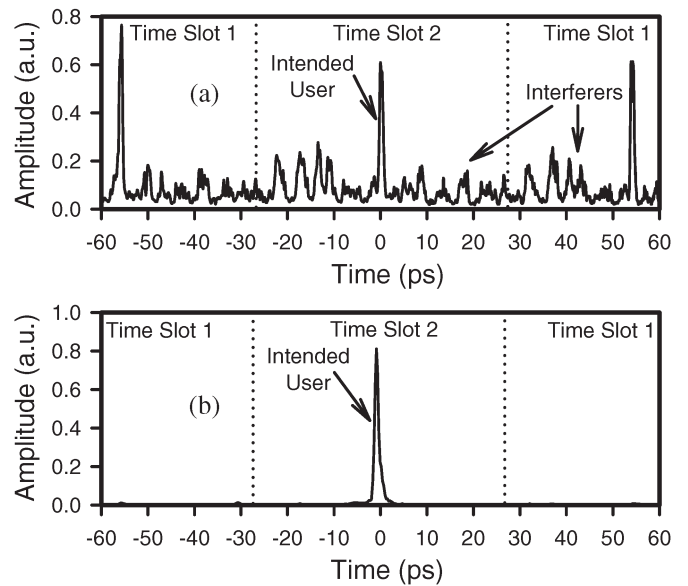

Fig. 4. Cross-correlation of the (a) input signal and (b) output signal of the NOLM with eight users in the testbed, each operating at 9 Gb/s. Time slot width is 55.5 ps and the cross-correlation reference pulse width is 400 fs.

recombine using a second piece of PM-DSF of identical length. This produces a linearly polarized output pulse, but its orientation will vary depending on whether the control pulse imparted the π phase shift. If present, the signal is gated and the pulse rotates by 90° with respect to the ungated pulse. A polarizer can then discriminate between the pulses by blocking the ungated pulses while passing the cross-polarized gated pulses and a filter can be used to block the control pulse. The UNI insertion loss (for the signal) was typically 15 dB and the suppression ratio for the switched and unswitched signal was approximately 7 dB.

When the UNI was positioned in front of the thresholder, the testbed was not able to attain a BER $< 10^{-9}$ for any number of users. The UNI output exhibited a pattern dependence that could be minimized by keeping the signal 6 dB below the control, but this forced the signal output to an unusably low level. Several other problems were apparent while trying to use the UNI as a gate including its polarization sensitivity, relatively wide window width of 6 ps, and sensitivity to any difference in PM-DSF lengths. Any mismatch reduced the contrast ratio and increased the signal loss. Ultimately, the severe decrease in optical signal-to-noise ratio (SNR) from the UNI kept it from being used in front of the thresholder.

When the UNI gate was moved in between the thresholder and the receiver, the testbed achieved error-free operation for up to six users. Unfortunately, with the UNI positioned after the thresholder, the advantage of blocking the interferer's energy is lost and the power requirements on the thresholder EDFA scale with the number of users. Section IV presents the BER data for this configuration.

The UNI performance (contrast ratio, window width, etc.) is lower than the best results achieved by other groups in simple demultiplexing experiments [23]. The best reported results list contrast ratios around 20 dB, a time gate width of $\sim$ 4 ps, and losses of < 6 dB (although this number is rarely stated). Since the UNI was implemented with available components from our lab, the setup was not fully optimized. However, after evaluating the results from the NOLM, we concluded that even

if the UNI was performing as well as the best reports, it would still be inferior as a time gate in the O-CDMA testbed.

B. NOLM Time Gate

The NOLM (Fig. 2) consists of a variable ratio coupler (VRC), a wavelength coupler (WC), 500 m of HNLF, and a control pulse at a wavelength other than the signal. The control pulse is created by amplifying the laser source's 400-fs pulses and then significantly broadening the pulses' spectrum through SPM in 1 km of DSF. The DSF output is filtered by a 1-nm bandpass filter centered at 1540 nm, resulting in a 3-ps pulse that is then amplified to an average power of +15 dBm for use with the NOLM. This is similar to using a separate wavelength channel (window) for control of network synchronization as demonstrated in [12]. The signal enters the VRC and splits into clockwise- and counterclockwise-propagating signals. Without the control pulse present, they each travel around the loop experiencing the same phase shift and recombine at the VRC. Since the net phase shift is zero, the entire signal will exit the input port of the VRC, thus acting as a mirror. To operate as a time gate, a control pulse is coupled into the loop through a WC and temporally aligned with the clockwise signal. As the control pulse copropagates with the clockwise signal in the HNLF, it imparts a phase shift to the signal via XPM. If the net phase shift is π, that portion of the signal exits from the output port of the VRC. Since the control pulse is at a different wavelength than the signal, it is separated from the signal by a long-pass filter at the output of the NOLM. The NOLM's 13 dB insertion loss is compensated by pre-NOLM and post-NOLM EDFAs. Typically, the NOLM's contrast for switched and unswitched pulses was 15–20 dB and the output pulse width was approximately 900 fs.

Fig. 4 shows time-domain data demonstrating the NOLM's performance. Fig. 4(a) is a cross-correlation of the input to the NOLM (400-fs reference pulse width) with the time scale

centered on the intended user's 55.5-ps-wide time slot (Time Slot 2). The intended user's pulse width is ∼ 900 fs and three interfering users are also visible in the user's, and both adjacent, time slots. Fig. 4(b) shows a cross-correlation of the output of the NOLM. Here, a single time slot (Time Slot 2) has been selected and nearly all of the energy from the interferers has been suppressed.

The superior performance of the NOLM with respect to the UNI led to its use as a time gate in the testbed. Specifically, the shorter gate width, lower loss, and relative simplicity made it the better choice.

IV. TESTBED EXPERIMENTAL RESULTS

The testbed was operated in two different configurations: one for taking data with the UNI time gate and the other with the NOLM time gate. Fig. 2 shows the NOLM time gate configuration, but the UNI time gate configuration is only slightly different, with the positions of the thresholder and the time gate reversed. For all of the measurements, the best results obtained are presented and each encoder consistently uses a particular code. Also, Encoder 1 with Walsh 5 is always the intended user so that these data can be compared with each other and our earlier results [10], [13]. Although these data do not include transmission experiments, it has recently been demonstrated that 500-fs pulses can be transmitted through 50 km of SMF-28 at 10 Gb/s with a combination of standard dispersion compensating fiber (DCF) and a pulse shaper (similar the those described in Section II) for final residual dispersion compensation [24].

A. UNI Time Gate Results

Fig. 5 shows the performance of the testbed with the UNI time gate placed after the nonlinear thresholder, and the total received power is measured at the input to the thresholder. As mentioned in Section III-A, the testbed was not able to obtain error-free operation for any number of users when the UNI gate preceded the thresholder. Also, these data were taken with the laser source operating at 10 Gb/s and the time MUX adjusted to create two 50-ps-wide time slots. The back-to-back data were taken with the time MUX and the encoders and the decoder removed. For the rest of the curves, the time MUX, encoders, and decoder are in place. Analyzing the 5-dB power penalty between the back-to-back and two-user curves, 3 dB arises from the addition of a second time slot and the rest is presumably due to spectral filtering and residual dispersion in the encoder and decoder. This causes the pulse to broaden and reduce its peak power, for a given average power, in the thresholder. Additional users are added by unblocking other encoders. With additional users, power sharing inside the saturated EDFA between the encoder and decoder as well as the thresholder EDFA results in an expected 3- and 1.8-dB penalty for the two-to-four user and four-to-six user cases, respectively. For the six-user curve, the accumulation of interfering users' power is great enough to generate some spectrum inside the thresholder, causing the slight reduction in the BER curve slope. However, all cases achieve error-free (BER $< 10^{-12}$) operation.
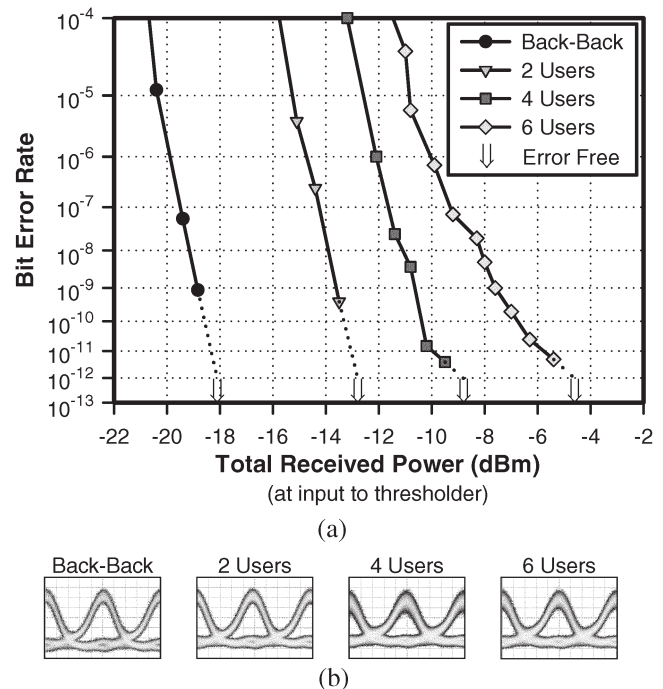

(a)

(b)

Fig. 5. (a) BER performance of the slotted SPECTS O-CDMA testbed with a UNI time gate and the testbed operating at 10 Gb/s/user. Total received power is measured at the input to the thresholder and the error-free point indicates the minimum power for BER $< 10^{-12}$. (b) Corresponding eye diagrams for BER curves shown in (a).

Valid arguments can be made for measuring the BER at several locations in the testbed. However, we chose to take the measurement at the input to the thresholder since it, along with the UNI time gate and O/E converter, can be considered to be the O-CDMA "receiver." Instead, if the testbed BER was measured just after the time gate, the BER curves would collapse with only a small power penalty as the number of users is increased. This is due to the time gate rejecting most of the interferers' energy and the fact that as interfering users are added, very little of their energy makes it through the thresholder. Fig. 6 presents BER data for the SPECTS O-CDMA testbed utilizing a UNI time gate. In this case, the O-CDMA receiver has the nonlinear thresholder preceding the UNI time gate and O/E converter. Fig. 6 demonstrates that the BER curves also collapse when the measurement location is at the input to the O/E converter. BER data were taken at the input to the O/E converter to show the minimization of the power penalties when compared to data taken at the input to the thresholder (see Fig. 5).

B. NOLM Time Gate Results

Fig. 7(a) shows the BER statistics of the testbed for a varying number of users, each operating at 9 Gb/s. The BER was measured versus the total input power to the DC-EDFA proceeding the NOLM. The back-to-back data were taken with the encoders and decoder bypassed, but with the NOLM and thresholder in place (Fig. 2). Then, with the encoders and decoder back in the testbed, we successively unblocked Encoders 1–4 to take the BER data for two, four, six, and eight users, respectively. The accompanying eye diagrams shown in
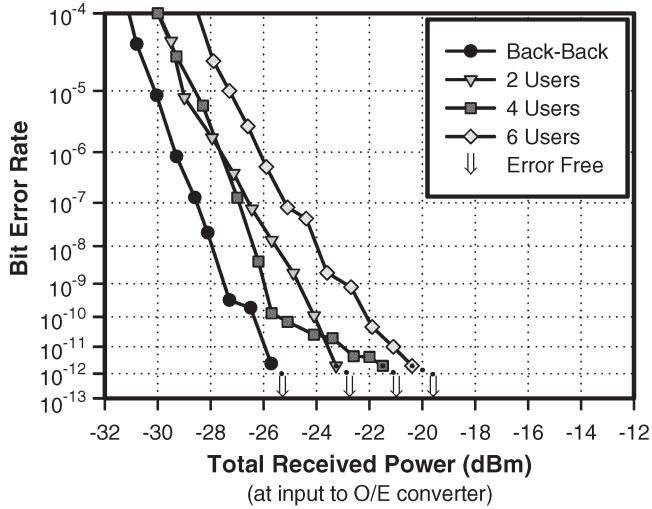
Fig. 6. Measured BER performance of the time-slotted SPECTS O-CDMA testbed operating at 10 Gb/s/user. The O-CDMA receiver is configured with the thresholder first, then UNI time gate and O/E converter. Total received power is measured at the input to the O/E converter and the error-free point indicates the minimum power for BER $< 10^{-12}$.
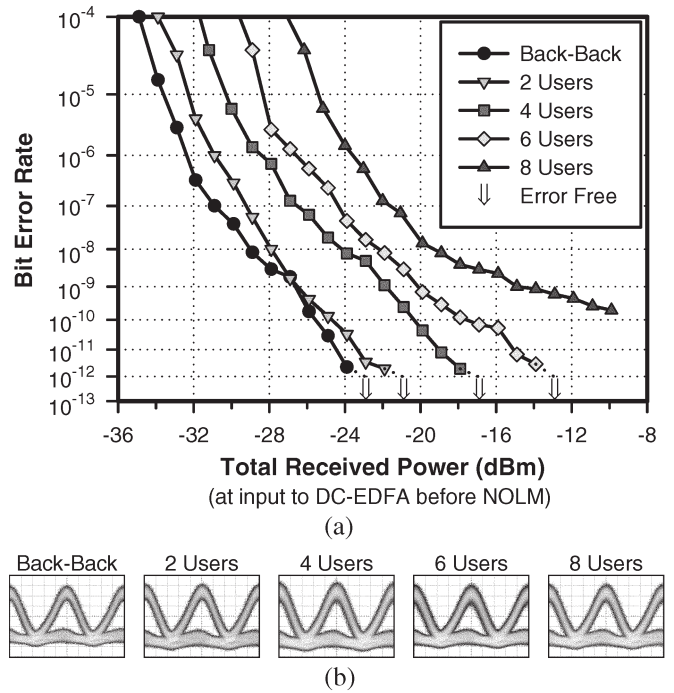

(a)

(b)

Fig. 7. (a) BER performance of the time-slotted SPECTS O-CDMA testbed with a NOLM time gate and the testbed operating at 9 Gb/s/user. Total received power is measured at the input to the DC-EDFA before the NOLM and the error-free point indicates the minimum power for BER $< 10^{-12}$. (b) Corresponding eye diagrams for BER curves shown in (a).

Fig. 7(b) were all taken at a total received power of approximately -10 dBm.

The $\sim$ 1-dB power penalty between back-to-back and two-user data arises from spectral filtering in the encoders and decoder and possibly some residual dispersion. The spectral filtering is due to the wavelength-dependent efficiency when coupling back into the collimators and results in an 8- to 10-nm bandwidth (FWHM). The power penalty of 3 dB between the two- and four-user curves is purely a consequence of power sharing within the EDFAs, thereby halving each user's power. The additional 0.5- to 1-dB power penalty is presumably due to MUI. Power sharing is responsible for 1.7 dB of the $\sim$ 2-dB power penalty between the four- and six-user curves, as is 1.2 dB of the 5-dB power penalty in the six- to eight-user case. The residual power penalty in both cases is mostly due to MUI. It did not matter which order the interfering users were added (e.g., Encoders $2 \rightarrow 3 \rightarrow 4$ versus Encoders $3 \rightarrow 4 \rightarrow 2$). The power penalties tended to be very consistent.

V. SIMULATIONS OF TESTBED PERFORMANCE

Numerical simulations of the SPECTS O-CDMA testbed have become an important part of evaluating and improving the testbed's performance. There are currently very few references [25] in the literature demonstrating realistic simulations of O-CDMA networks that include important effects such as EDFA gain shape and noise, wavelength-dependent component losses, nonlinear effects in fibers, and dispersion (i.e., optical layer transmission impairments). By taking advantage of the advanced models and the easily reconfigurable graphical layout available in RSoft's OptSim software, we have begun to explore these issues in our SPECTS O-CDMA testbed.

The testbed has four major components: the laser source with time MUX, encoders and decoder, time gate, and nonlinear thresholder. Each of these can be broken down into its various components and modeled in OptSim (Fig. 8). Currently, the laser source is modeled as a mode-locked laser with a

transform-limited 500-fs Gaussian output pulse. However, the testbed's laser source produces pulses that are much more complex owing to their generation from nonlinear fiber-based compression, resulting in a nonuniform pulse spectrum. This difference does lead to some discrepancies between simulations and measured results on the testbed. Included with the laser model is an additive noise source representing amplitude and phase noise of the laser. EDFA models include measured small signal gain with saturation effects and the measured *input power-dependent* amplified spontaneous emission (also wavelength dependent). The encoders and decoder are modeled by calls to MATLAB code followed by a filter model. The MATLAB code Fourier transforms the time waveform, impresses the phase code in the frequency domain, and then performs an inverse Fourier transform. The encoder model is fairly ideal, it does not yet include spectral resolution effects of the pulse shaper or phase nonuniformity across the LC-SLPM. Additional characterization of the LC-SLPM and pulse shaper will need to be completed before introducing these effects, but we have early indications that each spectral chip may be phase shifted by a value that is appreciably ($\sim$ 10%–20%) different from π. The encoder filter model is based on measurements of the filtering function for the current encoders. The NOLM time gate is realistically modeled including XPM in the nonlinear fiber that is used by the control pulse (3-ps Gaussian) to impart a phase shift on the clockwise-propagating signal (cf., Fig. 2). The nonlinear thresholder is one of the most difficult components to model. We have found that typical values for dispersion and the nonlinear coefficient from the manufacturer's data sheet do not have enough
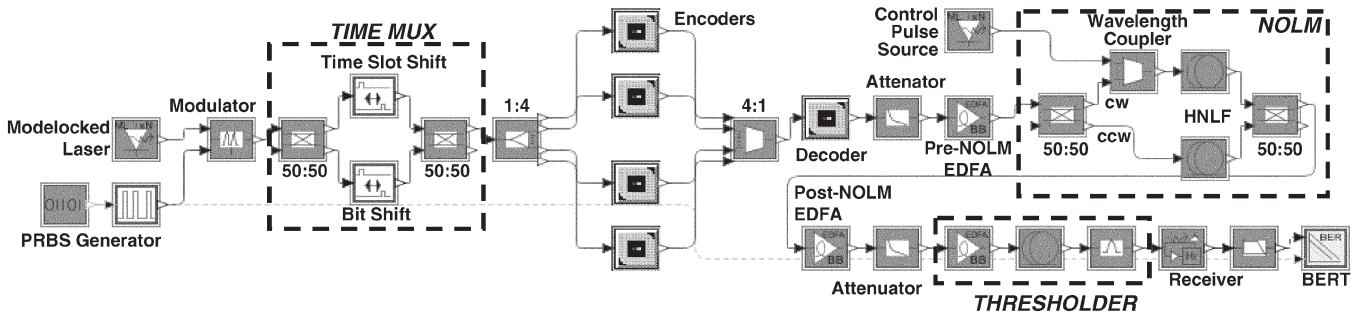
Fig. 8. Screen shot of the SPECTS O-CDMA testbed as modeled in OptSim showing only the essential elements used for the simulations.
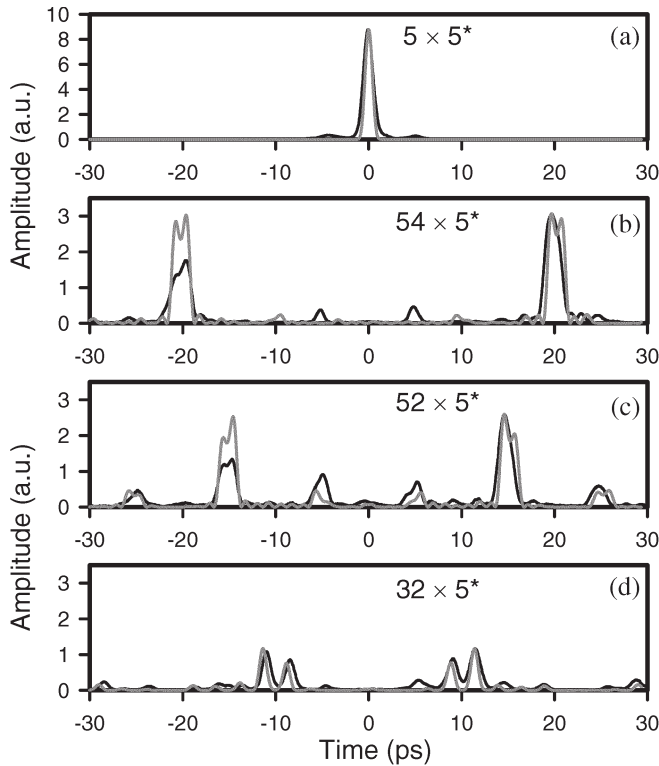

Fig. 9. Measured cross-correlation of the decoder output (black) overlayed with the corresponding simulation result (grey) for each individual channel. Decoded signal from (a) Encoder 1, (b) Encoder 2, (c) Encoder 3, and (d) Encoder 4. The upper right corner of each subfigure displays the relevant codes (see Table I) for the encoder and decoder (* indicates conjugate). The cross-correlation reference pulse width is 400 fs.
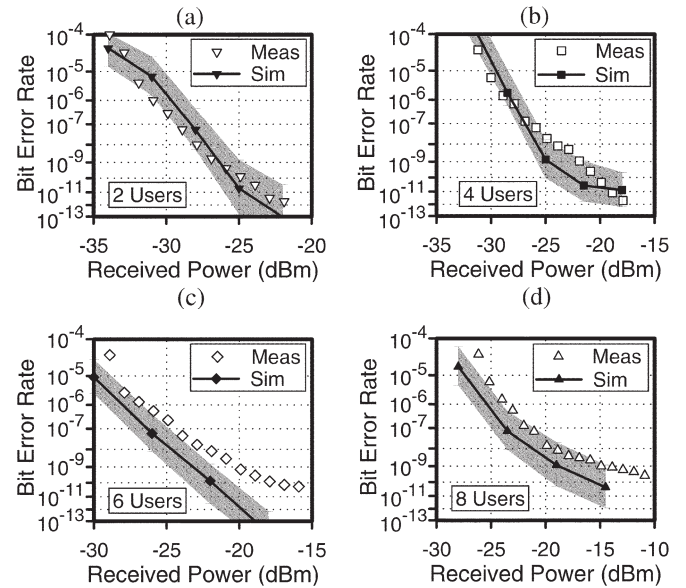

Fig. 10. Simulated BER performance of the time-slotted SPECTS O-CDMA testbed with a NOLM time gate for (a) two, (b) four, (c) six, and (d) eight users at 9 Gb/s/user. Total received power is measured at the input to the DC-EDFA before the NOLM. Measured data (white fill) from Fig. 7 are shown for reference. Grey shading indicates confidence limits for 2^7 simulated bits.

accuracy to correctly model the fiber. It is necessary to directly characterize the fiber through standard measurement techniques to achieve a reasonable match between simulations and measured data. Components such as the modulator, power splitters, and optical filters were modeled using parameters from the manufacturers' data sheets and were supplemented with lab measurements when required.

Fig. 9 shows the results of the encoder simulation model compared with the measured performance in the testbed. To make these measurements experimentally, the time MUX and all but one encoder were blocked (see Fig. 2). Then, using a cross-correlator, the output signal of the decoder was measured while the signals from Encoders 1–4 were successively passed through the decoder. Although the amplitude scales for each subfigure in Fig. 9 are arbitrary, they are kept to scale with one another. Also, simulation data do not include the effect

of cross-correlating the decoder output with a 400-fs pulse. Fig. 9(a) shows the correctly decoded output of Encoder 1. The measured output pulse is longer and has satellite pulses that the simulation does not predict. This is due in part to the simulation using a transform-limited Gaussian input pulse. Also, the simulation does not include the residual dispersion and phase nonuniformity that may exist in the encoders, but it does include the spectral filtering that occurs. Fig. 9(b) presents the incorrectly decoded output of Encoder 2 with some disagreement in the height of the peak at -20 ps and extra peaks at ± 5 ps. Both of these differences are likely caused by phase nonuniformity across the spectrum during encoding and decoding and/or differences in the real and simulated pulse spectrum shape. A reasonably good match between the measured and simulated incorrectly decoded output of Encoder 3 is apparent in Fig. 9(c). Again, there is a slight disagreement in the height of the peak at -15 ps due to phase nonuniformity and spectrum differences. Fig. 9(d) shows the simulated and measured incorrectly decoded outputs of Encoder 4.

Simulations of the BER statistics of the testbed were carried out for two, four, six, and eight users (Fig. 10). The mean calculated BER and associated BER confidence limits (grey

shading) [26], as determined by the number of bits (2^7) used in the simulation, are plotted with the measured BER. Sensitivity was mainly affected by the small signal gain of the pre-NOLM DC-EDFA. In order to fit the measured two-user BER within the confidence limits of the simulated BER, we had to adjust the gain by < 3 dB from the measured value, and the laser noise, which was unknown, was adjusted to set the BER floor at high received powers. Simulations were then run for four, six, and eight users. For six and eight users, the simulations predict better testbed performance than was measured. This is not unexpected since the simulations do not include every source of signal degradation such as the spurious reflections and nonuniform phase of the LC-SLPM or the laser pulse's temporal and spectral shape.

As the individual models for components in the testbed are refined through further characterization and testing, the accuracy of the overall simulations should improve to the point where predictions of the testbed performance under various stresses (e.g., transmission impairments, component degradation or power surges) can be determined. This is especially important as we try to realize more practical implementations of O-CDMA networks.

VI. CONCLUSION

This paper has successfully demonstrated a synchronous time-slotted spectral phase-encoded time-spreading (SPECTS) optical code division multiple access (O-CDMA) testbed that supports up to eight simultaneous users, each operating at 9 Gb/s. The testbed achieved error-free operation for up to six users and a bit error rate BER $< 10^{-9}$ for eight users. This was due, in part, to the effective suppression of multiuser interference (MUI) by the nonlinear optical loop mirror (NOLM) time gate and the highly nonlinear fiber (HNLF)-based nonlinear thresholder. This paper also presented a compact setup for concurrently encoding and decoding five channels using a single two-dimensional (2-D) liquid-crystal spatial light phase modulator (LC-SLPM). Performance of an alternative, but less effective, time gate based on a nonlinear interferometer (UNI) was shown for up to six users. OptSim was used to perform numerical simulations showing the operation and performance of the SPECTS O-CDMA testbed. The simulated time-domain data from the decoder output were in good agreement with the measured cross-correlations of the testbed's decoder output for each channel. Also, the measured BER generally fell within the confidence limits of the simulated BER statistics.

ACKNOWLEDGMENT

REFERENCES

[1] A. Stok and E. H. Sargent, "The role of optical CDMA in access networks," *IEEE Commun. Mag.*, vol. 40, no. 9, pp. 83–87, Sep. 2002.

[2] J. Shah, "Optical CDMA," *Opt. Photon. News*, vol. 14, no. 4, pp. 42–47, Apr. 2003.

[3] P. R. Prucnal, M. A. Santoro, and T. R. Fan, "Spread spectrum fiber-optic local area network using optical processing," *J. Lightw. Technol.*, vol. LT-4, no. 5, pp. 547–554, May 1986.

[4] J. A. Salehi, A. M. Weiner, and J. P. Heritage, "Coherent ultrashort light pulse code-division multiple access communication systems," *J. Lightw. Technol.*, vol. 8, no. 3, pp. 478–491, Mar. 1990.

[5] Z. Jiang, D. Seo, S.-D. Yang, D. E. Leaird, A. M. Weiner, R. V. Roussev, C. Langrock, and M. M. Fejer, "Spectrally coded O-CDMA system with four users at 2.5 Gbit/s using low power nonlinear processing," *Electron. Lett.*, vol. 40, no. 10, pp. 623–625, May 13, 2004.

[6] H. Sotobayashi, W. Chujo, and K. Kitayama, "Highly spectral-efficient optical code-division multiplexing transmission system," *IEEE J. Sel. Topics Quantum Electron.*, vol. 10, no. 2, pp. 250–258, Mar.–Apr. 2004.

[7] L. Tancevski and I. Andonovic, "Wavelength hopping/time spreading code division multiple access systems," *Electron. Lett.*, vol. 30, no. 17, pp. 1388–1390, Aug. 18, 1994.

[8] R. M. H. Yim, L. R. Chen, and J. Bajcsy, "Design and performance of 2-D codes for wavelength-time optical CDMA," *IEEE Photon. Technol. Lett.*, vol. 14, no. 5, pp. 714–716, May 2002.

[9] V. Baby, C. S. Bres, I. Glesk, L. Xu, and P. R. Prucnal, "Wavelength aware receiver for enhanced 2D OCDMA system performance," *Electron. Lett.*, vol. 40, no. 6, pp. 385–387, Mar. 18, 2004.

[10] V. J. Hernandez, Y. Du, W. Cong, R. P. Scott, K. Li, J. P. Heritage, Z. Ding, B. H. Kolner, and S. J. B. Yoo, "Spectral phase encoded time spreading (SPECTS) optical code division multiple access for terabit optical access networks," *J. Lightw. Technol.*, vol. 22, no. 11, pp. 2671–2679, Nov. 2004.

[11] Z. Jiang, D. Seo, S. Yang, D. Leaird, R. Roussev, C. Langrock, M. Fejer, and A. Weiner, "Four-user 10-Gb/s spectrally phase-coded O-CDMA system operating at $\sim$ 30 fJ/bit," *IEEE Photon. Technol. Lett.*, vol. 17, no. 3, pp. 705–707, Mar. 2005.

[12] S. Etemad *et al.*, "Spectrally efficient optical CDMA using coherent phase-frequency coding," *IEEE Photon. Technol. Lett.*, vol. 17, no. 4, pp. 929–931, Apr. 2005.

[13] R. P. Scott, W. Cong, K. Li, V. J. Hernandez, B. H. Kolner, J. P. Heritage, and S. J. B. Yoo, "Demonstration of an error-free 4 × 10 Gb/s multiuser SPECTS O-CDMA network testbed," *IEEE Photon. Technol. Lett.*, vol. 16, no. 9, pp. 2186–2188, Sep. 2004.

[14] H. P. Sardesai and A. M. Weiner, "Nonlinear fibre-optic receiver for ultrashort pulse code division multiple access communications," *Electron. Lett.*, vol. 33, no. 7, pp. 610–611, Mar. 1997.

[15] Z. Jiang, D. S. Seo, D. E. Leaird, A. M. Weiner, R. V. Roussev, C. Langrock, and M. M. Fejer, "Multi-user, 10 Gb/s spectrally phase coded O-CDMA system with hybrid chip and slot-level timing coordination," *IEICE Electron. Exp.*, vol. 1, no. 13, pp. 398–403, Oct. 10, 2004.

[16] J. P. Heritage, A. M. Weiner, and R. N. Thurston, "Picosecond pulse shaping by spectral phase and amplitude manipulation," *Opt. Lett.*, vol. 10, no. 12, pp. 609–611, Dec. 1985.

[17] A. M. Weiner, J. P. Heritage, and E. M. Kirschner, "High-resolution femtosecond pulse shaping," *J. Opt. Soc. Amer., B, Opt. Phys.*, vol. 5, no. 8, pp. 1563–1572, Aug. 1988.

[18] J. C. Vaughan, T. Feurer, and K. A. Nelson, "Automated two-dimensional femtosecond pulse shaping," *J. Opt. Soc. Amer., B, Opt. Phys.*, vol. 19, no. 10, pp. 2489–2495, Oct. 2002.

[19] N. S. Patel, K. A. Rauschenbach, and K. L. Hall, "40-Gb/s demultiplexing using an ultrafast nonlinear interferometer (UNI)," *IEEE Photon. Technol. Lett.*, vol. 8, no. 12, pp. 1695–1697, Dec. 1996.

[20] J. P. Sokoloff, P. R. Prucnal, I. Glesk, and M. Kane, "A terahertz optical asymmetric demultiplexer (TOAD)," *IEEE Photon. Technol. Lett.*, vol. 5, no. 7, pp. 787–790, Jul. 1993.

[21] J. H. Lee, P. C. Teh, P. Petropoulos, M. Ibsen, and D. J. Richardson, "A grating-based OCDMA coding-decoding system incorporating a nonlinear optical loop mirror for improved code recognition and noise reduction," *J. Lightw. Technol.*, vol. 20, no. 1, pp. 36–46, Jan. 2002.

[22] N. Wada, H. Sotobayashi, and K. Kitayama, "Error-free 100 km transmission at 10 Gbit/s in optical code division multiplexing system using BPSK picosecond-pulse code sequence with novel time-gating detection," *Electron. Lett.*, vol. 35, no. 10, pp. 833–834, May 13, 1999.

[23] C. Schubert, S. Diez, J. Berger, R. Ludwig, U. Feiste, H. G. Weber, G. Toptchiyski, K. Petermann, and V. Krajinovic, "160-Gb/s all-optical demultiplexing using a gain-transparent ultrafast-nonlinear interferometer (GT-UNI)," *IEEE Photon. Technol. Lett.*, vol. 13, no. 5, pp. 475–477, May 2001.

[24] Z. Jiang, S. D. Yang, D. E. Leaird, and A. M. Weiner, "Fully dispersion-compensated $\sim$ 500 fs pulse transmission over 50 km single-mode fiber," *Opt. Lett.*, vol. 30, no. 12, pp. 1449–1451, Jun. 15, 2005.

[25] H. X. C. Feng, A. J. Mendez, J. P. Heritage, and W. J. Lennon. (2000, Jul. 3). Effects of optical layer impairments on 2.5 Gb/s optical CDMA transmission. *Opt. Exp.* [Online]. *7(1)*, pp. 2–9. Available: http://www.opticsexpress.org/abstract.cfm?URI=OPEX-7-1-2

[26] *OptSim 4.5 Models Reference: Volume II Block Mode*, Ossining, NY: RSoft Design Group Inc., Physical Layer Division, 2005.

Ryan P. Scott received the B.S. degree in laser electrooptics technology from the Oregon Institute of Technology, Klamath Falls, in 1991, and the M.S. degree in electrical engineering from the University of California, Los Angeles (UCLA), in 1995. He is currently working toward the Ph.D. degree in electrical engineering from UCLA.

He is currently with the Laser Electro-Optic Research Group (LEORG) at the University of California, Davis (UC Davis). His research interests include temporal imaging, precise measurement of laser amplitude and phase noise, and the development of optical code division multiple access technology.
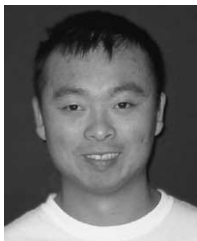
Wei Cong received the B.S. degree in physics from Jilin University, Changchun, China, in 1999, and the M.S. degree in applied science from the University of California, Davis (UC Davis), in 2002. He is currently working toward the Ph.D. degree in applied science at UC Davis.

He is currently a Graduate Student Researcher at the Laser Electro-Optic Research Group (LEORG), UC Davis. His research work includes optical communication and ultrafast pulse shaping.

Vincent J. Hernandez was born in San Francisco, CA, on 1976. He received the B.S. and M.S. degrees in electrical engineering from the University of California, Davis, in 1999 and 2004, respectively. He is currently working toward the Ph.D. degree in optical communications at the same university, conducting part of his research in conjunction with Lawrence Livermore National Laboratory.

His current interest lies in developing optical code division multiple access technology.

Kebin Li, photograph and biography not available at the time of publication.

Brian H. Kolner (S'79–M'85–SM'03) received the B.S. degree in electrical engineering from the University of Wisconsin, Madison, in 1979, and the M.S. and Ph.D. degrees in electrical engineering from Stanford University, Stanford, CA, in 1981 and 1985, respectively.

From 1985 to 1991, he was a Member of the Technical Staff at Hewlett-Packard Laboratories, Palo Alto, CA, and in 1991, he joined the Electrical Engineering Department at the University of California, Los Angeles (UCLA), and became Vice-Chairman for Undergraduate Affairs in 1993. At UCLA, he taught courses in microwave measurements, Fourier optics, and quantum mechanics, and conducted research on space–time duality and temporal imaging. In 1996, he moved to the University of California, Davis, where he holds joint appointments in the Departments of Applied Science and Electrical and Computer Engineering. His current research interests are in temporal imaging, laser phase and amplitude noise, and terahertz spectroscopy.

Dr. Kolner was awarded a David and Lucile Packard Foundation Fellowship in 1991, and served as a Guest Editor for the IEEE JOURNAL OF SPECIAL TOPICS IN QUANTUM ELECTRONICS in 1996 and 2003.
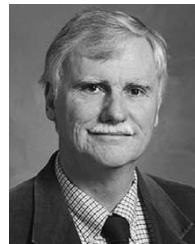
Jonathan P. Heritage (S'74–M'75–SM'89–F'90) received the M.S. degree in physics from the San Diego State University, San Diego, CA, in 1970 and the Ph.D. degree in engineering from the University of California, Berkeley, in 1975.

He was an Alexander von Humboldt Stiftung Postdoctoral Fellow at the Physics Department of the Technical University of Munich, Munich, Germany. From 1976 to 1984, he was a Member of the Staff at AT&T Bell Laboratories. In 1984, he joined the staff at the newly formed Bell Communications Research, where he became a Distinguished Member of Professional Staff. In July 1991, he joined the faculty of the Department of Electrical and Computer Engineering at the University of California, Davis (UC Davis). In 1999, he was awarded a joint appointment with the Department of Applied Science, UC Davis Livermore. He is currently a Professor of Electrical Engineering and Computer Science and a Professor of Applied Science at UC Davis. He is the author of more than 100 papers and eight patents, and has been an active researcher in picosecond and femtosecond quantum electronics and nonlinear optics for 29 years. His present research interests are in optical microelectromechanical systems, optical code division multiple access, and network issues, including device and link bit error rate modeling of wavelength division multiplexing networks. He also contributes to microphotonics for free-space optical switches and femtosecond pulse shaping. His interests range from nanostructures for photofield emission in vacuum to X-ray generation by Compton scattering for biomedical applications.

Prof. Heritage is a Fellow of the Optical Society of America (OSA) and the American Physical Society. He was a corecipient (with A. M. Weiner) of the 1999 IEEE/Lasers and Electro-Optics Society (LEOS) W. J. Streifer Award for Scientific Achievement. He was active in IEEE LEOS and is a past elected Member of the Board of Governors. He is the Co-Originator and Co-chair of the 1990 and 1992 IEEE LEOS/COMSOC Summer Topical Meeting on Optical Multiple Access Networks. He was the Technical Program Chair of the LEOS IEEE'94 Annual Meeting, a Member at Large for LEOS'95, and the General Chair for LEOS'96. He was the Program Chair of the 1999 24th International Conference on Infrared and Millimeter Waves. He was an Associate Editor of the IEEE JOURNAL OF QUANTUM ELECTRONICS and the IEEE PHOTONICS TECHNOLOGY LETTERS. He coedited the Special Issue on Ultrafast Optics and Electronics of the IEEE JOURNAL OF QUANTUM ELECTRONICS.

S. J. Ben Yoo (S'82–M'84–SM'97) received the B.S. degree in electrical engineering with distinction, the M.S. degree in electrical engineering, and the Ph.D. degree in electrical engineering with minor in physics from Stanford University, Stanford, CA, in 1984, 1986, and 1991, respectively.

Prior to joining Bellcore in 1991, he conducted research at Stanford University on nonlinear optical processes in quantum wells, a four-wave-mixing study of relaxation mechanisms in dye molecules, and ultrafast diffusion-driven photodetectors. During this period, he also conducted research on lifetime measurements of intersubband transitions and on nonlinear optical storage mechanisms at Bell Laboratories and IBM Research Laboratories, respectively. Prior to joining University of California at Davis (UC Davis) in 1999, he was a Senior Research Scientist at Bellcore, leading technical efforts in optical networking research and systems integration. His research activities at Bellcore included optical-label switching for the next-generation Internet, power transients in reconfigurable optical networks, wavelength interchanging cross connects, wavelength converters, vertical-cavity lasers, and high-speed modulators. He also participated in the advanced technology demonstration network/multiwavelength optical networking (ATD/MONET) systems integration, the OC-192 synchronous optical network (SONET) ring studies, and a number of standardization activities. He is currently a Professor of Electrical Engineering at UC Davis and the Director of UC Davis branch Center for Information Technology Research in the Interest of Society (CITRIS). His research at UC Davis includes high-performance all-optical devices, systems, and networking technologies for the next-generation Internet. In particular, he is conducting research on architectures, systems integration, and network experiments related to all-optical label switching routers and optical code division multiple access technologies.

Prof. Yoo is a Senior Member of the IEEE Lasers and Electro-Optics Society (LEOS) and a Member of the Optical Society of America (OSA) and Tau Beta Pi. He is the recipient of the Defense Advanced Research Projects Agency (DARPA) Award for Sustained Excellence in 1997, the Bellcore CEO Award in 1998, and the Mid-Career Research Faculty Award (UC Davis) in 2004. He also serves as an Associate Editor for IEEE PHOTONICS TECHNOLOGY LETTERS.